

# A structural modeling approach to the solid-solution materials based on the similar atomic environment

Fuyang Tian <sup>1,a</sup>, De-Ye Lin <sup>2,3,a</sup>, Hongquan Song<sup>1,4</sup>, Xingyu Gao <sup>3\*</sup>, Ya-Fan Zhao <sup>2,3†</sup>, and Hai-Feng Song <sup>3,2‡</sup>

1. Institute for Applied Physics, University of Science and Technology Beijing, Beijing 100083, China
2. Software Center for High Performance Numerical Simulation, China Academy of Engineering Physics, Beijing 100088, China
3. Institute of Applied Physics and Computational Mathematics, Beijing 100088, China
4. School of Physics, Normal University of Zhoukou, Zhoukou 466001, Henan province, China

**Abstract** Solid solution is an important way to enhance the structural and functional performances of materials. In this work, we develop a new structural modeling approach to solid-solution materials. Firstly, the description of atomic environment (AE) of an atom on sublattice in solid solution is introduced based on the concepts of atom cluster and lattice cluster. The average atomic environment of elements in the same sublattice for a certain supercell configuration could be calculated and the similarity to the desired fully disordered or short-range ordered (SRO) structure could be quantitatively evaluated. Based on the assumption that the structure model should have similar atomic environment (SAE) of the desired structure, the SAE approach is proposed by transferring the structural modeling for solid solution to an optimization problem in the configuration space. A new type of SRO parameter based on AE is introduced and the SRO could be naturally included in the SAE objective function, which could offer finer description of SRO in solid solution. Secondly, we pay efforts to enhance the practicality and functionality of this approach, including appropriate weight functions for atom clusters, implementation techniques in Metropolis Monte Carlo sampling, and support for all 230 space groups. Furthermore, the newly introduced SRO parameters are treated as constraints of the optimization problem to construct solid solution. Taking the typical quinary CoCrFeMnNi high-entropy alloy, continuous solid-solution binary TaW alloy and ternary CoCrNi medium-entropy alloy with SRO as prototypes, we apply our method in combination with *ab initio* calculations to investigate the structural properties and compare the calculated results with experiments.

**Key words:** similar atomic environment, solid solution, short-range order, high-entropy alloy, *ab initio* calculations

## I. Introduction

Solid-solution materials are typical disordered systems. The solid-solution alloys compose of at least two kinds of alloying elements and adopt a typical crystal structure, such as face centered cubic (fcc), body centered cubic (bcc), hexagonal close packed (hcp),  $L1_2$ ,  $L2_1$ , B2, NaCl, diamond and perovskite structures, etc. Solid solution is one of the fundamental methods to improve the mechanical strength, corrosion and oxidation resistance of structural materials and to modulate

---

<sup>a</sup> Have the same contribution to this work.

\* gao\_xingyu@iapcm.ac.cn

† zhao\_yafan@iapcm.ac.cn;

‡ song\_haifeng@iapcm.ac.cn;

energy band of functional materials. For example, the alloying Cr element (>13%) is responsible for the resistance against corrosion of stainless steel in various chemical environments [1]. The partial solid solution on sublattice site in  $L1_2$  phase is helpful to regulate  $Co_3(Al,W)$  as potential high-temperature structural material [2]. More recently, the high-entropy materials are basically solid solutions, including high-entropy alloy (HEA), high-entropy metallic glasses, high-entropy ceramics, high-entropy thermoelectric materials, and so on [3]. The high-throughput calculation or material gene engineering has been considered as an accelerator for the development of novel materials [4–7]. In high-throughput calculations, the electronic structure, phase stability, and intrinsically structural and functional properties could be obtained by using *ab initio* calculations based on density functional theory [8,9].

An *ab initio* calculation for complicated materials usually starts with the structural construction. Whereas, extending *ab initio* calculation to the system related to the presence of various kinds of disorder, especially for multi-component alloys, remains a difficult problem. The most common form of disorder is the breakdown of translational symmetry of crystal lattice sites. Two main categories of methods have been proposed to model the alloying induced disordered solid-solution phases. One is based on the effective medium theory, including the virtual lattice approximation (VCA) [10] and the coherent potential approximation (CPA) [11]. The other one is the finite-size supercell method, including the cluster expansion (CE) method [12], special quasi-random structure (SQS) method [13], and small set of ordered structures (SSOS) method [14]. The VCA adopts the oversimplified average of corresponding one-electron potential of alloying elements. Both electron potential and wave functions are not self-averaging quantities [15]. The one-site CPA method is based on the mean-field theory that can elegantly treat both chemical and magnetic disorders in fully disordered alloys at arbitrary composition, while the local atomic environment flux is ignored [16]. The SQS method is an approach to modeling the fully disordered solid solution via the objective function with the best possible small periodic supercell based on the CE theory. The SSOS is expected to use the finite SQS configurations to simulate the disordered structure of multicomponent alloys.

In solid solution, different atom sizes and bonding behaviors of alloying elements derived from solute elements produce unexpected local environments of solute atoms and solvent atoms, which may induce local lattice distortions and short-range order (SRO). These local environments may result in excellent properties in solid-solution materials. For example, the hardness of an alloy often increases with increasing atomic radius difference of alloying elements [17]. The SRO may play an important role in the low electronic and thermal conductivities of the equimolar CoCrNi solid-solution medium entropy alloy [18,19]. The different bonding behaviors of alloying elements may induce partial disorder in solid solution. For instance,  $L2_1$   $(NiCo)_2TiAl$  Heusler phase enhances creep resistance in multi-phase alloys [20,21] and the  $L1_2$   $Co_3(Al,W)$  is a potential high-temperature structural material [2,22]. With increase of Al content, the paramagnetic  $CoCrFeNiAl_x$  ( $x=0-2$ ) adopt the fcc structure ( $x < 0.60$ ) and the bcc structure ( $x > 1.23$ ), with an fcc-bcc duplex region in between the two pure phases at room temperature [23–25]. For the experimental investigation of solid solution, the atom size difference induced local lattice distortion and elastic modulus misfit are often measured via the pair distribution function (PDF) of atoms, which represents the local coordination of atom with its neighboring atoms [26]. However, as far as we know, there are few feasible *ab initio* calculation methods that could take into account the SRO effect properly, in principle, although the CE method can capture the SRO effect in random alloys [27].

In this work, we propose a new finite-size supercell based structural modeling approach to solid-solution materials. This approach is arising from the similar atomic environment (SAE) model in

which a similarity function is established to measure the similarity of any supercell configuration from its expectation. Then the structural modeling for solid-solution materials is transformed to an optimization problem in the configuration space. Besides, we also introduced a new type of SRO parameters, which could provide finer description of SRO. With the new parameters, the SRO can be naturally considered in the optimization problem. The comparison with the SQS method is studied and several implementation techniques are developed such that the SAE approach supports the modeling of solid-solution structures with fully disorder, partial disorder and short-range order. The effectiveness of this approach is shown by sufficient examples from cross validation with SQS and applications in three typical alloys.

In the following sections, we firstly discuss in details the concepts of lattice cluster and atom cluster, the description of atomic environment, the similarity function derived for the SAE model and accordingly the procedure to generate a solid-solution structure. The corresponding flowcharts of algorithms and procedures are shown. The comparisons of SAE and SQS approaches are also discussed. In the section of Application, taking the typical quinary CoCrFeMnNi HEA, continuous solid-solution binary TaW alloy and ternary CoCrNi medium-entropy alloy with the SRO as prototypes, we apply the SAE method in combination with *ab initio* calculations to investigate the structural properties and compare the calculated results with the available experiments. We end the paper with Conclusion.

## II. Methodology

### 1 Similar Atomic Environment (SAE) method

Before introducing the SAE method, we need to introduce three basic assumptions: 1). the atomic environment of an atom in solid solution could be described by the arrangement of its neighboring atoms. 2). In a certain sublattice, the atoms are independently identically distributed in fully disordered solid solution. 3). the optimal solid-solution model and the desired structure should have similar atomic environment (SAE). The SAE method is developed based on these three assumptions.

Based on assumption 1, the atomic environment (AE) of an atom is determined by its element type and neighboring atoms. Based on the cluster expansion theory [28], the AE of an atom could be decomposed to a series of atom clusters formed by the atom and its neighboring atoms. The AE could be quantitatively described by an array of the number of the atom clusters. Based on the assumption 2, the characteristic of the AE of atoms in fully disordered as well as short-range ordered solid solution could be derived. A similarity function is designed to evaluate the similarity between any given configuration and the desired solid solution. Finally, from assumption 3, the structural modeling of chemical disordered solid solution is transformed into the optimization problem in the configuration space.

We first discuss in detail how to characterize the chemical disorder in a supercell of solid-solution material. It is assumed that the supercell contains  $W$  different sublattices and there are  $N_i$  atoms with  $M_i$  types of elements in the  $i$ th sublattice. Further, we define the concepts about lattice cluster and atom cluster. The important notations are summarized in [Table 1](#).

**Table 1** Summary of basic notations and description in the SAE method.

Notation	Name	Description
$e_i^u$	element	the $u$ th element in the $i$ th sublattice
$c_i^u$	concentration	the concentration of the $u$ th element in the $i$ th sublattice
$X_{i,l}$	lattice site	the $l$ th lattice site in the $i$ th sublattice
$X_{i,l}^u$	atom	the $l$ th lattice site in the $i$ th sublattice being occupied by element $e_i^u$
$\sigma$	configuration of a supercell	two dimensional array to describe the configuration of a supercell, $\sigma_{i,l}$ is the element type of the atom occupied the $l$ th lattice site of the $i$ th sublattice
$G_2(\alpha_{i,l}, \beta_{j,m})$	binary lattice cluster	a binary lattice cluster formed by two lattice sites $\alpha_{i,l}$ and $\beta_{j,m}$
$ G_2(\alpha_{i,l}, \beta_{j,m}) _{\sigma}$	number of binary lattice clusters	the total number of $G_2$ clusters being equivalent to $G_2(\alpha_{i,l}, \beta_{j,m})$
$A_2(u, v)$	binary atom cluster	a binary atom cluster based on a $G_2$ lattice cluster $G_2(\alpha_{i,l}, \beta_{j,m})$ , formed by two atoms $\alpha_{i,l}^u$ and $\beta_{j,m}^v$
$ A_2(u, v) _{\sigma}$	number of binary atom clusters	total number of $A_2$ clusters being equivalent to $A_2(u, v)$ under configuration $\sigma$
$ A_2(u, v) _{\sigma}^{\alpha}$	number of binary atom cluster related to atom $\alpha$	total number of $A_2$ clusters being equivalent to $A_2(u, v)$ related to atom $\alpha$ under configuration $\sigma$
$G_3(\alpha_{i,l}, \beta_{j,m}, \gamma_{k,n})$	ternary lattice cluster	a ternary lattice cluster formed by three lattice sites $\alpha_{i,l}$ , $\beta_{j,m}$ and $\gamma_{k,n}$
$ G_3(\alpha_{i,l}, \beta_{j,m}, \gamma_{k,n}) _{\sigma}$	number of ternary lattice clusters	the total number of $G_3$ lattice clusters being equivalent to $G_3(\alpha_{i,l}, \beta_{j,m}, \gamma_{k,n})$
$A_3(u, v, w)$	ternary atom cluster	a ternary atom cluster based on $G_3$ lattice cluster $G_3(\alpha_{i,l}, \beta_{j,m}, \gamma_{k,n})$ , formed by three atoms $\alpha_{i,l}^u$ , $\beta_{j,m}^v$ and $\gamma_{k,n}^w$
$ A_3(u, v, w) _{\sigma}$	number of ternary atom clusters	the total number of ternary atom clusters being equivalent to $A_3(u, v, w)$ under configuration $\sigma$
$ A_3(u, v, w) _{\sigma}^{\alpha}$	number of ternary atom clusters related to atom $\alpha$	the total number of ternary atom clusters being equivalent to $A_3(u, v, w)$ under configuration $\sigma$ related to atom $\alpha$

The  $u$ th element in the  $i$ th sublattice is denoted as  $e_i^u$ , and its concentration is  $c_i^u$ . For each sublattice, we have  $\sum_{u=1}^{M_i} c_i^u = 1$ , ( $i=1, \dots, W$ ). For a substitutional solid solution, the coordinates of each lattice site in the supercell could be regarded as fixed, while the type of element occupied on each lattice site is random. The supercell configuration could be denoted by a two dimensional array

$\sigma$ , where  $\sigma_{i,l}$  is the element type of the  $l$ th lattice site in the  $i$ th sublattice. The  $l$ th lattice site in the  $i$ th sublattice is represented as  $X_{i,l}$ . If the element type of lattice site  $X_{i,l}$  is  $e_i^u$ , this atom is denoted as  $X_{i,l}^u$ .

Furthermore, we have the following definitions about the lattice cluster and atom cluster. A lattice cluster is formed by a number of lattice sites. A lattice cluster with  $p$  atoms is denoted as  $G_p$ . A binary lattice cluster formed by two lattice sites  $\alpha_{i,l}$  and  $\beta_{j,m}$  is denoted as  $G_2(\alpha_{i,l}, \beta_{j,m})$ . For two different  $G_2$  lattice clusters  $G_2(\alpha_{i,l}, \beta_{j,m})$  and  $G_2(\alpha_{i,l'}, \beta_{j,m'})$ , if a rotational operation matrix  $\mathbf{R}$  and a translation vector  $\mathbf{t}$  exist, so that  $\mathbf{R}\alpha_{i,l} + \mathbf{t} = \alpha_{i,l'}$  and  $\mathbf{R}\beta_{j,m} + \mathbf{t} = \beta_{j,m'}$ , then the two lattice clusters are considered to be equivalent. Cluster  $G_2(\alpha_{i,l}, \beta_{j,m})$  could be considered as a representative of its equivalent clusters. The total number of equivalent  $G_2(\alpha_{i,l}, \beta_{j,m})$  in the supercell is denoted as  $|G_2(\alpha_{i,l}, \beta_{j,m})|_{\sigma}$ . The size of  $G_2$  is measured by the distance  $r$  between its two lattice sites, denoted as  $d(G_2)$ . Notation  $G_p^q$  is used to denote the  $q$ th lattice cluster with  $p$  atoms.

The arrangement of neighboring lattice sites around a certain lattice site is part of its atomic environment. Under a certain configuration  $\sigma$ , the number of equivalent  $G_2(\alpha_{i,l}, \beta_{j,m})$  lattice clusters containing the lattice site  $\alpha_{i,l}$  is denoted as  $|G_2(\alpha_{i,l}, \beta_{j,m})|_{\sigma}^{\alpha}$ . In solid-solution structure, both  $|G_2(\alpha_{i,l}, \beta_{j,m})|_{\sigma}^{\alpha}$  and  $|G_2(\alpha_{i,l}, \beta_{j,m})|_{\sigma}$  are fixed numbers being determined by the symmetry of the crystal structure and the size of the supercell, regardless of the configuration  $\sigma$ . For example, for the bcc structure, each atom has eight nearest neighboring atoms, so for the lattice cluster formed by an atom and one of its first nearest neighboring atoms,  $|G_2(\alpha_{i,l}, \beta_{j,m})|_{\sigma}^{\alpha}$  is eight.  $|G_2(\alpha_{i,l}, \beta_{j,m})|_{\sigma}$  is proportional to the number of atoms in the  $i$ th sublattice and  $|G_2(\alpha_{i,l}, \beta_{j,m})|_{\sigma}^{\alpha}$ . We have

$$|G_2(\alpha_{i,l}, \beta_{j,m})|_{\sigma} = \rho_i(\alpha_{i,l}, \beta_{j,m}) N_i |G_2(\alpha_{i,l}, \beta_{j,m})|_{\sigma}^{\alpha} \quad (1)$$

where  $\rho_i$  is the coefficient related to the composition of  $G_2$  cluster, depending on the cluster is being shared by how many atoms in the  $i$ th sublattice.

The lattice clusters could be further classified by the atom type in each lattice site. We further define an atom cluster  $A_p^{q,s}(u_s, v_s, w_s, \dots)$  as the  $s$ th atom cluster in  $G_p^q$ , with the lattice sites being occupied by  $u_s, v_s, w_s, \dots$  atoms. For instance, we define  $A_2(u, v)$  as a binary atom cluster based on the lattice cluster  $G_2(\alpha_{i,l}, \beta_{j,m})$ , formed by two atoms  $\alpha_{i,l}^u$  and  $\beta_{j,m}^v$ . Different combinations of  $(u, v)$  lead to different types of  $A_2$  atom clusters. Under a certain configuration  $\sigma$ , the number of equivalent  $A_2(u, v)$  cluster containing atom  $\alpha_{i,l}^u$  is denoted as  $|A_2(u, v)|_{\sigma}^{\alpha}$ , and the total number of equivalent  $A_2(u, v)$  clusters is denoted as  $|A_2(u, v)|_{\sigma}$ . For  $|A_2(u, v)|_{\sigma}^{\alpha}$  and  $|A_2(u, v)|_{\sigma}$ , we have

$$\lambda_{i,j}^{u,v} \rho_i(\alpha_{i,l}, \beta_{j,m}) \sum_{l, \sigma_{i,l}=e_i^u} |A_2(u, v)|_{\sigma}^{\alpha} = |A_2(u, v)|_{\sigma} \quad (2)$$

The  $\lambda_{i,j}^{u,v}$  is a parameter to avoid miss counting situation of atom clusters. If  $i = j$  and  $u$  differs from  $v$ , we have  $\lambda = 2$ , otherwise  $\lambda = 1$ .

The number of  $|A_2(u, v)|_{\sigma}$  and  $|G_2(\alpha_{i,l}, \beta_{j,m})|_{\sigma}$  satisfies

$$\sum_{A_2(u,v)} |A_2(u,v)|_{\sigma} = |G_2(\alpha_{i,l}, \beta_{j,m})|_{\sigma} \quad (3)$$

Similarly, the ternary lattice cluster  $G_3(\alpha_{i,l}, \beta_{j,m}, \gamma_{k,n})$  and ternary atom cluster  $A_3(u, v, w)$  could be defined. The three interatomic distances of  $(\beta_{j,m}, \gamma_{k,n})$ ,  $(\gamma_{k,n}, \alpha_{i,l})$  and  $(\alpha_{i,l}, \beta_{j,m})$  are denoted as  $r_1$ ,  $r_2$  and  $r_3$ . The size of  $G_3$  is defined as  $d(G_3)$ , which is equal to the maximum value of  $r_1$ ,  $r_2$ , and  $r_3$ . The notations of  $|G_3(\alpha_{i,l}, \beta_{j,m}, \gamma_{k,n})|_{\sigma}$ ,  $|G_3(\alpha_{i,l}, \beta_{j,m}, \gamma_{k,n})|_{\sigma}^{\alpha}$ ,  $|A_3(u, v, w)|_{\sigma}$  and  $|A_3(u, v, w)|_{\sigma}^{\alpha}$  could also be defined following similar manner.

The AE of atom  $\alpha_{i,l}^u$  could be described by a set of atom cluster  $\{A_p^{q,s}(u, u_2^s, \dots, u_p^s)\}$  containing  $\alpha_{i,l}^u$ , where  $A_p^{q,s}(u, u_2^s, \dots, u_p^s)$  means the  $s$ th atom cluster of the  $q$ th lattice cluster with  $p$  lattice sites, formed by elements  $u, u_2^s, \dots$  etc. The AE of atom  $\alpha_{i,l}^u$  could be exactly described by a three dimensional array

$$AE(\sigma, \alpha_{i,l}^u) = \left\{ |A_p^{q,s}(u, u_2^s, \dots, u_p^s)|_{\sigma}^{\alpha} \right\}_{p,q,s} \quad (4)$$

Eq. (4) means that the number of atom cluster  $A_p^{q,s}(u, u_2^s, \dots, u_p^s)$  in the atomic environment is  $|A_p^{q,s}(u, u_2^s, \dots, u_p^s)|_{\sigma}^{\alpha}$ . The AE array in eq. (4) could be used to describe the atomic environment of an atom in ordered and disordered structure. With proper choice of atom clusters, the AE of an atom in the non-crystalline structure could also be described. The AE array described in eq. (4) may be treated as a fingerprint or descriptor of an atom, which can be used in the classification of atoms or machine learning for solid solution.

It is obvious that for ordered structure, each atom in the same sublattice has identical AE. For disordered solid solution, the AE of each atom differs significantly because of the random distribution of elements in each sublattice. It is almost impossible to find a random structure in which the AE of each atom in a sublattice is identical. However, the statistical average of AE should be similar to the desired solid solution. The average AE for  $e_i^u$  atoms in the  $i$ th sublattice is described as

$$AE(\sigma, e_i^u) = \left\{ \sum_{l, \sigma_{i,l}=e_i^u} \frac{|A_p^{q,s}(u, u_2^s, \dots, u_p^s)|_{\sigma}^{\alpha}}{N_i C_i^u} \right\}_{p,q,s} \quad (5)$$

From eq. (2), we have that

$$AE(\sigma, e_i^u) = \left\{ \frac{|A_p^{q,s}(u, u_2^s, \dots, u_p^s)|_{\sigma}^{\alpha}}{\lambda_p^{q,s} \rho_i N_i C_i^u} \right\}_{p,q,s} \quad (6)$$

The above equation shows that the average AE of the  $e_i^u$  atoms in the  $i$ th sublattice is determined by the numbers of different types of atom clusters related to  $e_i^u$  atoms. The overall AE can be obtained by traversing each kind of element in each sublattice.

For fully disordered solid solution, based on the assumption that the atoms are independently identically distributed in the sublattice, the probability of finding atom cluster  $A_p^{q,s}(u_1^s, \dots, u_p^s)$  in all  $G_p^q$  is

$$P(A_p^{q,s}(u_1^s, \dots, u_p^s)) = \lambda_p^{q,s} \prod_{i=1}^p c_{u_i^s} \quad (7)$$

The expectation of  $|A_p^{q,s}(u_1^s, \dots, u_p^s)|_{\sigma}$  is

$$E(|A_p^{q,s}(u_1^s, \dots, u_p^s)|_{\sigma}) = \lambda_p^{q,s} \prod_{i=1}^p c_{u_i^s} |G_p^q|_{\sigma} \quad (8)$$

The expectation of the average AE for  $e_i^u$  atoms in the  $i$ th sublattice is

$$E(AE(\sigma, e_i^u)) = \left\{ \left( \prod_{i=2}^p c_{u_i^s} \right) |G_p^q|_{\sigma}^{\alpha} \right\}_{p,q,s} \quad (9)$$

A series of parameters based on the atom clusters could be defined to measure the degree of disorder of solid solution

$$\theta_p^{q,s} = \frac{E(|A_p^{q,s}(u_1^s, \dots, u_p^s)|_{\sigma})}{\lambda_p^{q,s} \left( \prod_{i=1}^p c_{u_i^s} \right) |G_p^q|_{\sigma}} \quad (10)$$

In fully disordered solid solution, we have  $\theta_p^{q,s} = 1$  for each kind of atom cluster. For structure with SRO, the atoms in the sublattice are no longer independent identically distributed. So the values of  $\theta_p^{q,s}$  are no longer equal to 1. The parameters  $\theta_p^{q,s}$  could be used to describe the SRO.

The popular Warren-Cowley SRO parameters are commonly used to describe the deviation of a solid-solution structure from fully disordered structure, usually defined as  $\alpha_n(A, B) = 1 - P_n(B, A) / c_A$ , where  $P_n(B, A)$  is the probability of finding A atoms in the  $n$ th nearest neighbor of B atoms, and  $c_A$  is the concentration of A atoms in solid solution. If a binary  $G_2^n$  lattice cluster is formed by a lattice sites and its  $n$ th nearest neighboring sites, and  $A_2(A, B)$  is the first atom cluster in  $G_2^n$  lattice cluster, we have  $\alpha_n(A, B) = 1 - \theta_2^{n,1}$ . The Warren-Cowley parameter is equivalent to  $\theta_p^{q,s}$  when  $p=2$ . Since the new SRO parameters are able to describe the SRO induced by interactions among multiple atoms, finer SRO description could be achieved.

The deviation of the average AE of  $e_i^u$  atoms from the expectation could be measured by

$$\Delta AE(\sigma, e_i^u) = \left\{ \theta_p^{q,s} - \frac{|A_p^{q,s}(u_1^s, \dots, u_p^s)|_{\sigma}}{\lambda_p^{q,s} c_i^u \left( \prod_{i=2}^p c_{u_i^s} \right) |G_p^q|_{\sigma}} \right\}_{p,q,s} \quad (11)$$

Considering all atom clusters  $A_p^{q,s}$  belonging to  $G_p^q$ , the standard deviation of the AE from the expectation is

$$\Delta_{G_p^q}(\sigma) = \sqrt{\frac{1}{N_A(G_p^q)} \sum_{A_p^{q,s}} \left( \theta_p^{q,s} - \frac{|A_p^{q,s}(u_1^s, \dots, u_p^s)|_{\sigma}}{\lambda_p^{q,s} \left( \prod_{i=1}^p c_{u_i^s} \right) |G_p^q|_{\sigma}} \right)^2} \quad (12)$$

A similarity function could be designed to quantitatively measure the similarity from given configuration  $\sigma$  to the expectation by

$$f(\sigma) = \sum_{G_p^q} \Delta_{G_p^q}(\sigma) \quad (13)$$

where  $N_A(G_p^q)$  is the number of types of atom clusters in lattice cluster  $G_p^q$ . The closer  $f(\sigma)$  is to 0, the more similar the AE is to the desired solid solution. Taking eq. (13) as the objective function, the problem of structural modeling of chemical disordered solid solution is transformed to a mathematical optimization problem in the configuration space. It should be noted that the SRO is naturally considered in the objective function.

## 2. Theoretical comparison with the SQS method

The SQS method is one of the most popular supercell methods applied in structural modeling for the chemical disordered materials [27]. We feel obliged to clarify the relationship between the SAE and SQS methods.

**Proposition:** for any configuration  $\sigma$ , if its SAE objective function is 0, the configuration must be an optimal configuration for the SQS method.

Our proof is as follows:

For a lattice cluster  $G_2(\alpha_{i,l}, \beta_{j,m})$ , the correlation function defined in the SQS method is reformulated as

$$\rho_{G_2}(\sigma) = \left\langle \Gamma_{A_2(u,v)}(\sigma) \right\rangle_{G_2} = \frac{\sum \Gamma_{A_2(u,v)}(\sigma)}{|G_2(\alpha_{i,l}, \beta_{j,m})|_{\sigma}}, \quad (14)$$

where  $\Gamma_{A_2(u,v)}(\sigma)$  is a cluster function. The summation in eq. (14) is over all possible atom clusters in the supercell.

Since equivalent atom clusters have the same cluster functions, eq. (14) is simplified as

$$\rho_{G_2}(\sigma) = \sum_{(u,v)} \frac{|A_2(u,v)|_{\sigma}}{|G_2(\alpha_{i,l}, \beta_{j,m})|_{\sigma}} \Gamma_{A_2(u,v)}(\sigma). \quad (15)$$

From the above formula, it is obvious that the correlation function is solely determined by the numbers of  $A_2(u, v)$  clusters in the supercell. For the fully disordered structure, the atoms in the sublattice are independently and identically distributed. So the correlation function could be calculated as

$$\rho_{G_2}(\sigma^{md}) = \sum_{(u,v)} \lambda_{i,j}^{u,v} c_i^u c_j^v \Gamma_{A_2(u,v)}(\sigma), \quad (16)$$

where the definition of  $\lambda_{i,j}^{u,v}$  is the same to eq. (2).

The SQS deviation function between a finite supercell configuration and fully disordered solid solution is defined as

$$\Delta\rho_{G_2}(\sigma) = \rho_{G_2}(\sigma) - \rho_{G_2}(\sigma^{md}) = \sum_{E_2(u,v)} \left( \frac{|A_2(u,v)|_{\sigma}}{|G_2(\alpha_{i,l}, \beta_{j,m})|_{\sigma}} - \lambda_{i,j}^{u,v} c_i^u c_j^v \right) \Gamma_{A_2(u,v)}(\sigma). \quad (17)$$

When the SAE objective function is 0, for each kind of atom clusters, we have

$$1 - \frac{|A_2(u,v)|_{\sigma}}{\lambda_{i,j}^{u,v} c_i^u c_j^v |G_2(\alpha_{i,l}, \beta_{j,m})|_{\sigma}} = 0 \quad (18)$$

Comparing eq. (17) and eq. (18), it is obvious that for any structure whose SAE objective function is 0, its SQS deviation function is also 0. The conclusion also holds for  $G_3$  and lattice clusters with more lattice sites.

However, the inverse proposition does not hold. For a configuration whose SQS deviation function is 0, its SAE objective function may not be 0. We found a counterexample structure as a proof. For an equimolar bcc binary AB solid solution, its lattice constant of unit cell is assumed to be 1.0. For a  $3 \times 3 \times 3$  supercell with 54 atoms, if the cutoff radii for  $G_2$  and  $G_3$  clusters are set to be 1.05, there are two types of  $G_3$  clusters. For the larger  $G_3$  lattice cluster, the three interatomic distances are 1.0, 1.0 and 1.0 and there are 54 equivalent  $G_3$  clusters in the supercell. For the  $A_3$  (A, A, A) atom cluster, the expectation of  $|A_3(A, A, A)|_{\sigma}$  is  $E(|A_3(A, A, A)|_{\sigma}) = 0.5^3 \times 54 = 6.75$ , which is not an integer. Meanwhile, for any supercell configuration  $\sigma$ ,  $|A_3(A, A, A)|_{\sigma}$  must be an integer. This leads to an intrinsically non-zero objective function for any  $\sigma$ . However, there are configurations whose SQS deviation function for this  $G_3$  cluster is 0, and the SAE objective function is larger than 0. In the SQS method, the value of the cluster function could be negative, so the summation of the deviations may cancel each other, leading to  $\Delta\rho_G(\sigma) = 0$ . The counterexample will also be shown in Section III.

Comparing with the SQS method, evaluation of the SAE objective function does not require the calculation of the cluster function. As a result, the implementation of the SAE method is much easier than the SQS method. The optimal SAE supercell configuration is also optimal for SQS method, while the inverse proposition does not hold. From the above discussion, we have proved that the SAE method is different from SQS, and the SAE method offers an alternative approach for structural modeling of solid solution other than SQS.

### III. Implementation

Based on the SAE method described in section II, we have developed a software package for the structural modeling of solid-solution materials. The periodic boundary condition (PBC) is strictly considered. In the present SAE model, thermodynamics is ignored, which is also adopted by the SQS method. In order to make the SAE software package more practical, several new functions are also implemented for the modeling of complicated solid-solution materials.

#### 1. Improvement in the objective function

With the objective function defined in eq. (13), the modeling of solid solution could be transformed to an optimization problem. The consideration of  $G_2$  and  $G_3$  lattice clusters are adequate for solid-solution structure modeling[27,29], furthermore, the lattice clusters with smaller size are more important for the properties of materials. Two cutoff radii  $r_{c2}$  and  $r_{c3}$  for the size of  $G_2$  clusters and  $G_3$  clusters are set. Only clusters whose sizes are smaller than the given cutoff radii are considered. The third improvement is to introduce weight in the objective function. In order to give the small lattice clusters larger weight, the objective function in eq. (13) is redesigned as

$$f(\sigma; r_{c2}; r_{c3}) = \sum_{d(G_2) < r_{c2}} w_{G_2}(r) \Delta_{G_2}(\sigma) + \sum_{d(G_3) < r_{c3}} w_{G_3}(r_1, r_2, r_3) \Delta_{G_3}(\sigma), \quad (19)$$

where  $r$  and  $r_1, r_2, r_3$  are the interatomic distances of  $G_2$  and  $G_3$ , respectively, and  $w_{G_2}$  and  $w_{G_3}$  are specific weights function for  $G_2$  and  $G_3$ . The weight functions should be designed such that the weight of small cluster is larger than the big cluster.

A candidate weight function is presented here. For all  $G_2$  considered in the objective function, the shortest  $r$  is defined as  $r^0$ . For a  $G_2$  with the interatomic distance being  $r$ , its weight in the objective function  $w_{G_2}(r)$  is defined as

$$w_{G_2}(r) = \frac{\exp(-r/r^0)}{\sum_{r'} \exp(-r'/r^0)}, \quad (20)$$

where  $r'$  is the interatomic distance between two lattice sites in a  $G_2$  cluster and the summation is over all kinds of  $G_2$ .

Similarly, for  $G_3$  clusters, the smallest interatomic distances ( $r_1, r_2, r_3$ ) in all  $G_3$  clusters are defined as ( $r_1^0, r_2^0, r_3^0$ ). The weight function is defined as

$$w_{G_3}(r_1, r_2, r_3) = \frac{\exp(-r_1/r_1^0) \exp(-r_2/r_2^0) \exp(-r_3/r_3^0)}{\sum_{r'_1, r'_2, r'_3} \exp(-r'_1/r_1^0) \exp(-r'_2/r_2^0) \exp(-r'_3/r_3^0)}, \quad (21)$$

where  $r'_1, r'_2, r'_3$  are the interatomic distances in  $G_3$  lattice clusters and the summation is over all kinds of  $G_3$  lattice clusters. With the implementation of weight function, the small clusters contribute more in the objective function.

In the Alloy Theoretic Automated Toolkit (ATAT) [27] package, the objective function for the SQS method is implemented as

$$Q = -wL + \sum_{G \in A} \Delta\rho_G(\boldsymbol{\sigma}) \quad (22)$$

where  $L$  is the largest  $l$  for such that  $\Delta\rho_G(\boldsymbol{\sigma})=0$  for all clusters  $G$  whose cluster sizes  $d(G) \leq l$ . With such feature, the deviation of small clusters should be optimized first. From the definition of  $L$ , we can see that the objective function will have a sharp drop if a structure if a larger  $l$  is found. We suggest that our weighted objective function is a better approach, since small change in the configuration will not induce dramatic change in the objective function.

## 2. Optimization of the objective function

For a finite supercell, the size of configuration space grows exponentially with the number of atoms in the supercell, which makes it impossible to traverse all configurations to find the configuration with the smallest objective function. In our implementation, the objective function is optimized by using the Metropolis Monte Carlo (MMC) algorithm, which is also used by the ATAT package and has also been shown to be efficient in structure prediction of atom clusters and crystal structure [30,31]. Given a configuration of the random configuration  $\boldsymbol{\sigma}_s$  as a seed, the objective function is evaluated as  $f(\boldsymbol{\sigma}_s)$ . A new configuration  $\boldsymbol{\sigma}_{\text{new}}$  is generated by randomly swapping the element types of two lattice sites in the same sublattice. The objective function of  $\boldsymbol{\sigma}_{\text{new}}$  is reevaluated as  $f(\boldsymbol{\sigma}_{\text{new}})$ . The seed is then updated by the Metropolis selection rule:

If  $f(\boldsymbol{\sigma}_{\text{new}}) < f(\boldsymbol{\sigma}_s)$ , the seed is updated to  $\boldsymbol{\sigma}_{\text{new}}$ . Otherwise a random value  $p$  is sampled in  $(0, 1)$  and compared with  $e^{(f(\boldsymbol{\sigma}_s) - f(\boldsymbol{\sigma}_{\text{new}})) / (k_B T)}$ , where  $k_B T$  is a user-specified parameter to adjust the acceptance ratio. If  $p < e^{(f(\boldsymbol{\sigma}_s) - f(\boldsymbol{\sigma}_{\text{new}})) / (k_B T)}$ , the seed  $\boldsymbol{\sigma}_s$  is updated to  $\boldsymbol{\sigma}_{\text{new}}$ . In other cases, the seed will not be updated. The procedure will be repeated for many times, until the objective function converges to a preset criterion, or the maximum number of structures has been achieved. Since the MMC algorithm is a relatively local method, and the optimized structure may be strongly influenced by

the quality of the initial seed. In our implementation, a certain number of random configurations are generated and evaluated by the objective function. The most optimal random configuration is chosen as the seed for the MMC optimization. The evolution procedure should be repeated for several iterations.

In the current implementation of the SAE method, the two atoms to be swapped in the MMC step are randomly selected. If the atomic environment of each atom is analyzed, the atoms whose atomic environment is far from the fully disordered state should be chosen with higher priority.

Using the MMC algorithm, the SAE objective function is efficiently optimized. The desired finite size supercell to model the disordered solid solution is obtained when the objective function converged.

### 3. Implementation of space group symmetry

In practice, the symmetry and composition of the solid-solution materials may be more complicated than the bcc, fcc and hcp phases. In the implementation of the SAE method, we have created a database for Wyckoff positions of all 230 space groups. In this database, the multiplicity, symbol, coordinates for each Wyckoff position and the possible translation vector of the space group is recorded. With this database, the SAE method supports the modeling of multi-component and multi-sublattice solid-solution materials of any space group symmetry.

In some materials with multiple sublattices, such as high-entropy ceramics and perovskite, the atoms in the system are partially disordered. There might be a sublattice in the system, the lattice sites in which are occupied by just one type of element. The generation of partial disordered system is naturally supported by the SAE method. For the fixed sublattice, the ratio of the element could be set to 1, the required partial disordered structure could be generated using the SAE method.

The SAE method is also able to generate structures for the interstitial solid-solution. For the interstitial solid solution, multiple types of sublattices could be defined, one for the solvent atoms and the others for the interstitials. The interstitial lattice sites are occupied by alloying atoms and vacancies. Once the sublattices and element concentrations are set, the structural modeling could be performed using the SAE method.

Furthermore, the input for the SAE method could also be greatly simplified. For example, in the  $Im\bar{3}m$  (#229) space group, we suppose that there are two different sublattices in the crystal structure, Wyckoff positions  $a$  and  $b$ , and the total number of atoms in a unit cell is eight. If no space group symmetry is used, all coordinates of the eight atoms should be supplied as the input for SAE method. When the space group symmetry is used, only two representative coordinates for Wyckoff position  $a$  and  $b$  need to be supplied, and all other 6 coordinates could be generated by space group symmetry operations.

### 4. Structural modeling with SRO as external constraints

By introducing  $\theta_p^{q,s}$  as SRO parameters, the objective function eq. (13) can be employed for the structure modeling of materials with SRO. However, the values of  $\theta_p^{q,s}$  are mutually dependent, making it difficult to calculate all  $\theta_p^{q,s}$  accurately. For instance, in a ternary ABC alloy, the values of  $\theta_2(A,A)$  will also influence the value of  $\theta_2(A,B)$  and  $\theta_2(A,C)$ , and may also influence the values of  $\theta_3(A,A,A)$ ,  $\theta_3(A,A,B)$ ,  $\theta_3(A,A,C)$  and so on. Here we introduce an alternative method to include

SRO in the structure modeling by treating the SRO parameters as external constraints.

In the implementation of SAE, a series of SRO parameters  $\theta_p^{q,s}$  could be supplied as external constraints. For each SRO parameter  $\theta_p^{q,s}$ , a minimum value  $\theta_p^{q,s,\min}$  and a maximum value  $\theta_p^{q,s,\max}$  are supplied. Using the SRO parameter  $\theta_p^{q,s}$ , the SRO related to atom cluster composed of more than three atoms could also be considered. An SRO objective function is designed as

$$\varepsilon(\sigma) = \sum_{\theta_p^{q,s}} \left| \frac{|A_p^{q,s}(u, v_s, \dots)|_{\sigma}}{\lambda_p^{q,s} c_i^u \prod c_{v_s} |G_p^q|_{\sigma}} - \frac{\theta_p^{q,s,\min} + \theta_p^{q,s,\max}}{2} \right| \quad (23)$$

The SRO objective function  $\varepsilon(\sigma)$  could also be effectively optimized by the MMC algorithm described in the previous section. The optimization terminates if all SRO parameters are inside the given ranges.

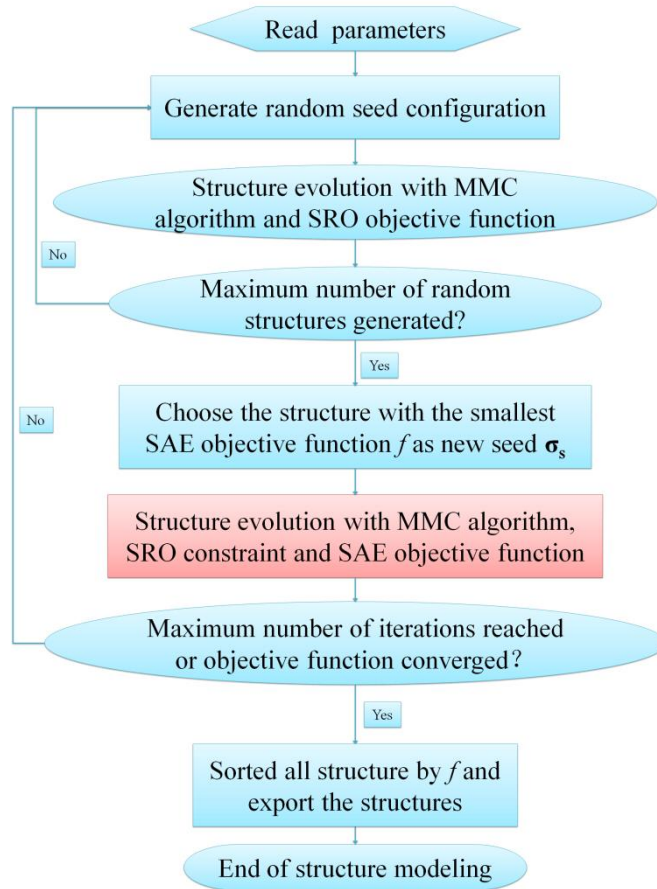


Fig. 1. Flowchart of the SAE method.

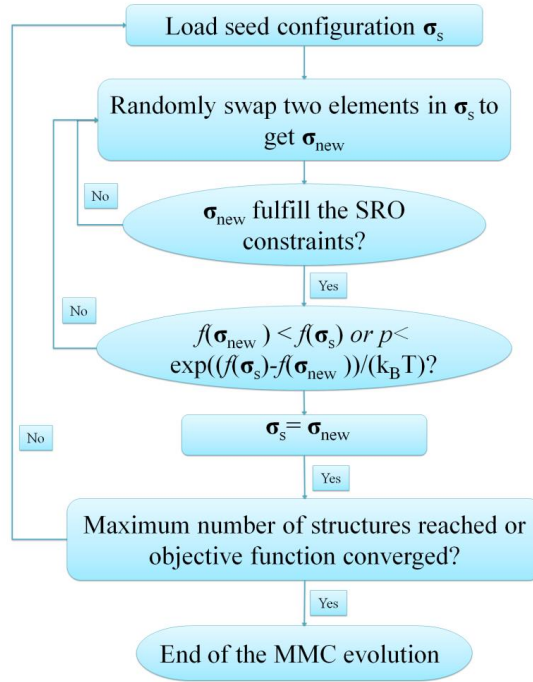


Fig. 2. Flowchart of the MMC algorithm with SRO constraints

Once the structure that fulfills all SRO constraints is generated, the structure will be further optimized according to the SAE objective function eq. (19). With SRO constraints, the SRO parameters will be checked in each MMC step. Only structures that fulfill the SRO constraints will be chosen as seeds in the optimization procedure. In this approach, we are able to get the most disordered configurations that fulfill the external SRO constraints.

Figure 1 shows the flowchart of the SAE structure generation. The part of the MMC algorithm with constraints is marked in red, which is further illustrated in Fig. 2. Note that for the SAE generated configurations with SRO constraints, the validated structure should be further determined by the free energy calculation or experiment observation.

In all, depending on the local atomic environments in real alloys, we can apply the SAE method to generate the solid-solution structure with fully disorder, partial disorder, short range order as well as the solid-solution structures with interstitials.

## 5. Numerical cross validation of SAE and SQS methods

Numerical comparison between the SQS and SAE methods is performed using four types of solid-solution structures, *i.e.* equimolar binary AB alloy and ternary ABC alloy for bcc and fcc phases. Structural models are generated using both SQS and SAE methods. The same-size supercell and the same cluster cutoff radii are used. We considered the  $G_2$  lattice cluster (two-body correlation) and  $G_3$  lattice cluster (three-body correlation) in both methods. The mcsqs program in the ATAT package is used as the implementation of SQS method [27].

For the bcc(fcc) structures, the lattice constants of the unit cell are  $a=b=c=1.0$ . A  $3\times 3\times 3$  supercell with 54 (108) atoms is used. The distances from any atom to its first and second nearest neighboring atoms are  $\sqrt{3}/2$  ( $\sqrt{2}/2$ ) and 1.0 (1.0), respectively. The cutoff radii for  $G_2$  and  $G_3$  clusters are set as 0.90 (0.75) for one test case, and 1.05 (1.05) for the other test case.

For both SAE and SQS methods, the MMC algorithm is applied to optimize the objective functions. We limited the maximum number of configurations to be 100,000 in each test run for

both methods. For each combination of composition and cutoff radii, the calculation will be repeated for three times, and only the best structures in the three runs are reported here. For the SAE method, the 10,000 configurations are divided to 10 iterations. 1000 random configurations are generated and evaluated in each iteration, and the configuration with the smallest objective function is chosen as the seed configuration for the MMC stage. The rest 9000 configurations are generated in the MMC stage. It is not guaranteed that the optimal structure could be obtained within limited MMC steps.

**Table 2** Comparisons between the present SAE method and the SQS method for the typical binary and ternary alloys. The derivations  $\Delta_{G_2}$  and  $\Delta_{G_3}$  are from Eqs (6) and (7), and  $\Delta_2$  and  $\Delta_3$  are the summation of difference of the two-body correlation and three-body correlation in the SQS method, respectively.

Symmetry	Composition	Cutoff	SAE Structure				SQS Structure			
			$\Delta_{G_2}$	$\Delta_{G_3}$	$\Delta_2$	$\Delta_3$	$\Delta_{G_2}$	$\Delta_{G_3}$	$\Delta_2$	$\Delta_3$
bcc	AB	0.9	0.000	0.000	0.000	0.000	0.000	0.000	0.000	0.000
		1.05	0.006	0.019	0.012	0.000	0.006	0.019	0.012	0.000
	ABC	0.9	0.000	0.000	0.000	0.000	0.000	0.000	0.000	0.000
		1.05	0.000	0.000	0.000	0.000	0.000	0.169	0.000	0.024
fcc	AB	0.75	0.000	0.000	0.000	0.000	0.000	0.000	0.000	0.000
		1.05	0.000	0.005	0.000	0.000	0.000	0.005	0.000	0.000
	ABC	0.75	0.000	0.000	0.000	0.000	0.000	0.008	0.000	0.003
		1.05	0.000	0.007	0.000	0.013	0.011	0.063	0.017	0.046

The optimal configurations generated by SQS and SAE methods are then further cross evaluated by the objective function of SAE and the summation of deviations of the SQS methods, respectively. The deviations of the optimal configurations generated by using the SAE and SQS methods are listed in **Table 2**.

For the bcc structures, when the cutoff radii are set to be 0.90, only one kind of  $G_2$  cluster (two-correlation function) is considered in SAE (SQS) methods. No  $G_3$  clusters (three-correlation functions) are considered because even the smallest  $G_3$  cluster has an interatomic distance of 1.0. Under such circumstance, both SAE and SQS methods are able to generate configurations with objective function being 0 during the tests. As we can see from **Table 2**, for all SAE configurations with  $\Delta_{G_2}=0$ , the  $\Delta_2$  values are all zero.

For the fcc AB and ABC structures with cutoff radii being 0.75, one  $G_2$  cluster and one  $G_3$  cluster are considered in the both methods. The SAE method is also able to generate configuration with objective function being 0 for AB and ABC alloys during the tests. However, the SQS method failed to generate perfectly matched configuration for ternary ABC alloy during the tests, due to the limited number of configurations or unreasonable seed configuration in the test runs.

When the cutoff radii for  $G_2$  and  $G_3$  clusters increase to 1.05, more lattice clusters are included in the objective functions of two methods. For the bcc binary AB alloy, the qualities of SAE structure and SQS structure are identical. Interestingly, though for both structures the  $\Delta_3$  values calculated by SQS method are 0, the corresponding  $\Delta_{G_3}$  values in the SAE method are larger than 0, showing that the SAE method is different from SQS. This is the counterexample we have mentioned in Section II. For the bcc ternary ABC alloy, the SAE method successfully generates configurations whose objective function is 0, while a configuration whose  $\Delta_{G_3}$  or  $\Delta_3$  is 0 is not obtained using SQS.

For the fcc ternary ABC alloy, the SAE method is able to generate configurations with  $\Delta_{G_2} = 0$  and a very small  $\Delta_{G_3}$ . Meanwhile, the configuration produced by the SQS method also has small  $\Delta_{G_2}$  and  $\Delta_{G_3}$ , but these values are larger than those of the SAE configurations. For the fcc AB alloy, we

also notice that for both configurations the  $\Delta_3$  values are 0, but the  $\Delta_{G3}$  values are larger than 0. This is one more counterexample showing that a perfectly matched SQS configuration is not sufficient for the SAE objective function to be 0.

Although different objective functions are adopted, the SAE method is comparable with the SQS method. The cross comparison suggested that any optimal configuration generated by SAE is sufficiently optimal for SQS.

## IV. Application

### 1. *Ab initio* calculation details

Based on the SAE methods, we have constructed supercell models for several typical solid-solution alloys and performed *ab initio* calculations to investigate their phase stabilities, so as to demonstrate the validity of SAE method.

In the present *ab initio* calculations, we employed the Vienna *Ab initio* Simulation Package (VASP) computer program [32] based on the density functional theory [8,9]. The exchange-correlation potentials were treated by the Perdew-Burkey Ernzerhof [33] functional within the generalized gradient approximation. The electron-ion interaction was described by the projector augmented wave (PAW) method [34]. The plane-wave cutoff energy is 300 eV. The Brillouin zone sampling was performed using the special  $k$  points generated by Monkhorst-Pack scheme [35] with density parameters  $0.2 \text{ \AA}^{-1}$ . The convergence tolerance level is  $10^{-6}$  eV for total energy and  $0.01 \text{ eV/\AA}$  for the max force on each atom, respectively.

In the calculations of ferromagnetic Co-Cr-Fe-Mn-Ni alloys, opposite spin moments are set for Cr, Mn atoms and Fe, Co, Ni atoms, *i.e.*, Cr and Mn are set as spin up, while Fe, Ni and Co are set as spin down. The paramagnetic state above the Curie temperature is modeled by using the disordered local moment (DLM) approximation [36]. Namely, the spin-up and spin-down atoms with equal atomic fraction for the same elements are treated as different atomic species distributed randomly in the supercell. For example, for a 180-atom CoCrFeMnNi quinary equimolar alloy, the SAE structure with PM state contains 10 components  $(18\text{Co}\uparrow 18\text{Co}\downarrow)(18\text{Cr}\uparrow 18\text{Cr}\downarrow)(18\text{Fe}\uparrow 18\text{Fe}\downarrow)(18\text{Mn}\uparrow 18\text{Mn}\downarrow)(18\text{Ni}\uparrow 18\text{Ni}\downarrow)$ .

### 2. Phase stability of CoCrFeMnNi alloy

As a typical HEA sample, single phase CoCrFeMnNi [37] alloy has drawn much attention since being reported in 2004. The experimental lattice parameter of fcc structure is about  $3.590\sim 3.610 \text{ \AA}$ , the corresponding equilibrium volume is  $11.56\sim 11.76 \text{ \AA}^3/\text{atom}$ . As far as we know, the experimental CoCrFeMnNi HEA was defaulted as the paramagnetic (PM) state, due to the heat treatment. The alloying elements adopt different magnetic states in their ground state: ferromagnetic (FM) for Fe, Ni, Co, and antiferromagnetic for Cr, and multi-magnetic for Mn. In the following section, the FM state represents the ferromagnetic set for Fe, Ni, Co, Mn and antiferromagnetic set for Cr, while AM state stands for antiferromagnetic set for Cr, Mn and ferromagnetic set for Fe, Ni, and Co in our *ab initio* calculations. For the PM state, the DLM approximation was employed. For the no magnetic (NM) state, we considered non spin polarized set in *ab initio* calculations.

Using the SAE method, we constructed a 180-atom supercell to model the disordered solid-solution structure, *i.e.*  $3\times 3\times 5$  fcc SAE structure (see Fig.3 A). The equilibrium volume predicted by

*ab initio* calculations is  $11.07 \text{ \AA}^3/\text{atom}$  for FM state,  $11.06 \text{ \AA}^3/\text{atom}$  for PM state, and  $11.04 \text{ \AA}^3/\text{atom}$  for AM state, respectively. They are slightly smaller than the experimental results, but agree well with the available results from the CPA calculations ( $10.98 \text{ \AA}^3/\text{atom}$  [38] and  $11 \text{ \AA}^3/\text{atom}$  [39]). Recent *ab initio* calculations suggested that hcp is more stable than fcc at  $T=0 \text{ K}$  [38,39], which agrees with more recent experiments [40,41]. To estimate the validity of SAE method for the phase stability, we constructed the hcp based SAE structure, *i.e.*  $5 \times 5 \times 3$  hcp supercell with 150 atoms (see Fig.3 B). From Table 2, we can find that at each magnetic state, the 150-atom hcp SAE structure is indeed more stable than the 180-atom fcc SAE structure in the ground state.

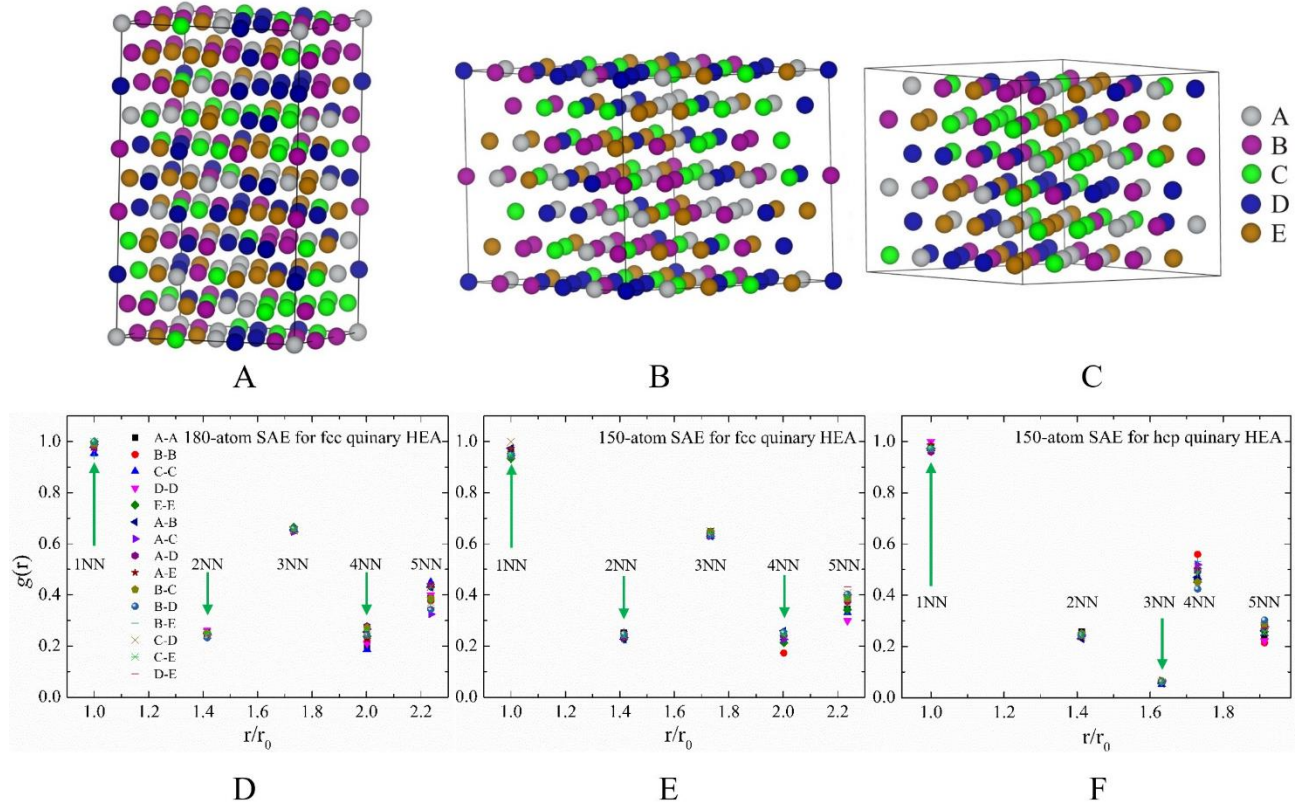


**Fig. 3.** SAE structures (A, B, C) and the corresponding radial distribution function  $g(r)$  (D, E, F) as a function of the 1NN-5NN atom pairs.  $r_0$  is the first neighboring atom distance. A and D for 180-atom fcc SAE structure, B and E for 150-atom fcc SAE structure based on ABC stacked configuration implemented along the fcc  $\langle 111 \rangle$  crystal direction, and C and E for 150-atom hcp SAE structure.

**Table 2** Equilibrium volume per atom  $V$  ( $\text{\AA}^3$ ), energy per atom  $E$  (eV/atom), and the magnetic moment per atom  $\mu$  ( $\mu_b$ ) for the different magnetic states (ferromagnetic FM, antiferromagnetic AM, paramagnetic PM, and no magnetic (without spin polarized set) NM) of fcc and hcp CoCrFeMnNi.

HEA	$V$ (180) fcc	$E$	$\mu$	$V$ (150) fcc $\langle 111 \rangle$	$E$	$\mu$	$V$ (150) hcp	$E$	$\mu$
FM	11.07	-7.781	0.58	10.07	-7.781	0.51	10.93	-7.802	0.22
AM	11.06	-7.783	0.37	10.07	-7.783	0.41	10.90	-7.794	0.15
PM	11.04	-7.780	0.03	11.01	-7.781	0.07	10.87	-7.791	0.09
NM	10.69	-7.751	0	10.69	-7.754	0	10.67	-7.786	0

In order to eliminate error caused by size effect, we then constructed the SAE structure with the same atom number to model the hcp and fcc CoCrFeMnNi HEA. Along the fcc $\langle 111 \rangle$  crystallographic direction, we constructed ABC stacked hexagonal structure and enlarged the 3-atom fcc $\langle 111 \rangle$  hexagonal structure to a 150-atom fcc $\langle 111 \rangle$  SAE structure, *i.e.*  $5 \times 5 \times 3$  supercell

(see Fig.3 C). From Table 2, we can see that the 150-atom hcp SAE structure is still more stable than the 150-atom fcc  $\langle 111 \rangle$  SAE structure. Interestingly, both *ab initio* predicted average energies per atom and the equilibrium volumes of fcc SAE and fcc $\langle 111 \rangle$  SAE structures are excellently consistent with each other for different magnetic states. For fcc SAE and fcc  $\langle 111 \rangle$  SAE structures, the total magnetic moment per atom at the FM state is very close to that of the AM state. Whereas the magnetic moment of PM state is close to zero, which may suggest the validity of DLM approximation application to the SAE method.

Figure 3 (D, E, F) shows the radial distribution function of the three SAE structures above. The quinary alloy has 15 different types of atom pairs. Due to the equimolar ratio of alloying elements, the radial distributions are very close to each other for the 1th to 5th nearest neighboring atom pairs.

### 3. Partial disorder of Ta-W alloy

From the fully ordered phase to the fully disordered phase, there often exists the partial disordered phase. For an equimolar binary alloy with B2 structure, it has two different sublattices (*A* and *B*). Taking binary Ta-W alloy as an example, we use the concentration of W ( $x$ ) located on the *A* lattice site to define the partial disorder in the Ta-W alloy. When  $x=0$ , Ta (W) occupies the *A* (*B*) lattice sites, the Ta-W alloy form a fully ordered B2 phase. Whereas  $x=0.5$ , Ta and W are uniformly distributed on *A* and *B* lattice sites, and the Ta-W alloy forms a random solid solution with bcc crystal structure. The partial disorder is corresponding to the value  $x$  ( $0 < x < 0.5$ ).

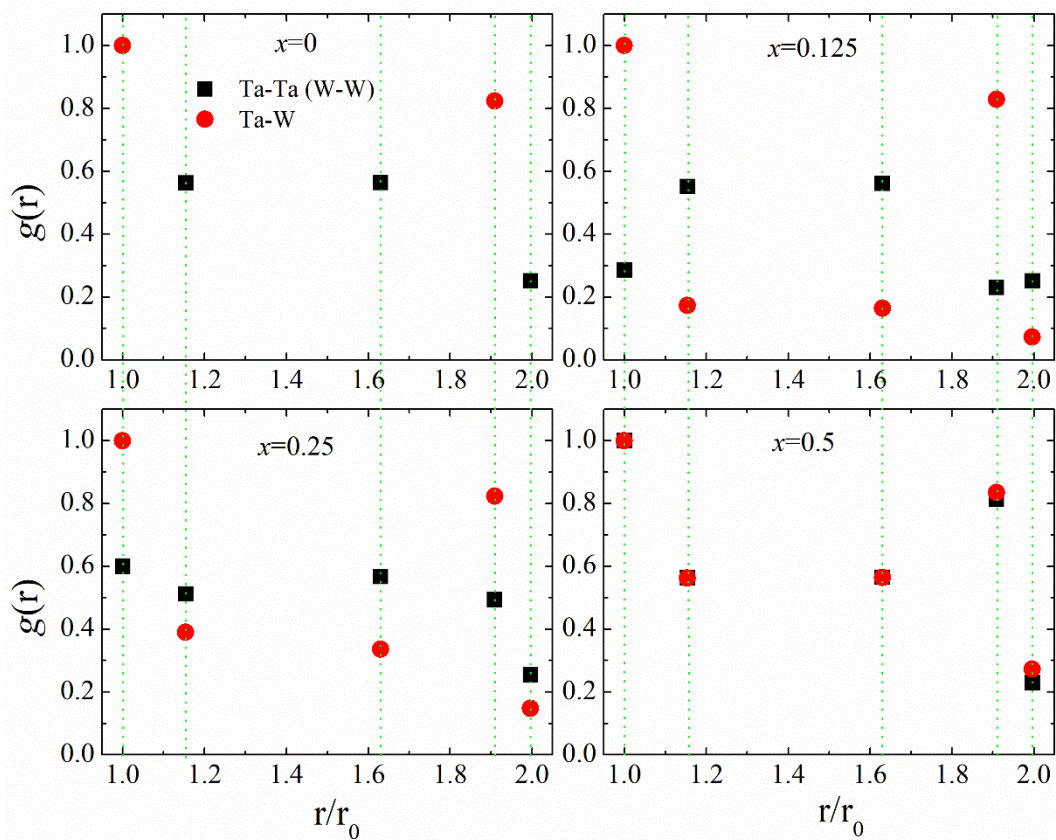


Fig. 4. Radial distribution  $g(r)$  as a function of the nearest neighboring atom pairs  $N=1-5$  for the 54-atom SAE Ta-W alloys from fully order B2 ( $x=0$ ) to partial disordered ( $x=0.125, 0.25$ ) to fully disordered bcc ( $x=0.5$ ).  $r_0$  is the first nearest neighboring atom distance.

**Figure 4** shows the radial distribution  $g(r)$  as a function of the nearest neighboring (NN) atom pairs. The  $g(r)$  of the first nearest neighboring (1NN) atom pairs is normalized as 1. The 1NN atom number is set as  $n_0$ . We define the  $N$ th nearest neighboring atom distance and atom number as  $r$  and  $n$ , respectively. The  $g(r)$  of the  $N$ th nearest neighboring atom pairs satisfies  $g(r) = (n/n_0) \times (r_0/r)^2$ . For example, in the bcc crystal structure with lattice parameter  $a_0$ , with respect to the 1NN atom distance, the 2NN and 3NN atom distances should be equal to  $(\sqrt{3}a_0/2)/a_0 \sim 1/1.155$  and  $(\sqrt{3}a_0/2)/(\sqrt{2}a_0) \sim 1/1.633$ , respectively. When  $x=0$ , Ta and W form the fully ordered B2 structure. The 1NN atom pairs are all Ta-W. The number of 1NN atom pairs should be 8. The 2NN atom pairs are Ta-Ta or W-W. The number of the 2NN (3NN) atom pairs is 6 (12). When the 1NN atom number is normalized, the radial distribution of the 2NN (3NN) atom pair is equal to  $g(r) = (6/8) \times (1/1.155)^2 = 0.562$  ( $(12/8) \times (1/1.633)^2 = 0.563$ ).

From **Fig. 4**, we see that the atom pair (W-W, Ta-W or Ta-Ta) orderly occupies on the nearest neighboring, whereas the Ta-Ta, W-W and Ta-W atom pairs exist in the bcc phase and they have similar radial distribution from 1NN to 5NN atom pairs. For the partial disordered phase, the radial distribution of Ta-W atom pair is not equal to that of Ta-Ta and W-W atom pairs. The number of atom pairs depends on the different nearest neighboring environments. With increase of W concentration  $x$ , the number of Ta-W atom pairs become close to Ta-Ta (W-W) atom pairs. **Table 3** lists the energy difference of Ta-W alloys. The energy difference becomes larger with increase of disorder degree (from the fully ordered B2 to fully disordered bcc). It suggests that the stable phase of Ta-W alloy tends to form the ordered B2 structure at  $T = 0$  K.

**Table 3** Listed are the energy differences  $\Delta E$  (meV/atom) of Ta-W binary alloy, the partial disorder is represented by the content  $x$  (0, 0.125, 0.25, 0.5) of alloying element W occupying on A lattice in B2 crystal structure. The reference energy is that of B2 Ta-W alloy.

Ta-W	Sub lattice (A, B)	$\Delta E$
B2	A-Ta1.00W0.0, B-Ta0.0W1.0	0.00
↓	A-Ta0.875,W0.125, B-Ta0.125,W0.875	9.73
	A-Ta0.75,W0.25, B-Ta0.25,W0.75	16.18
bcc	A, B-Ta0.5,W0.5	21.77

#### 4. Short-range order in CoCrNi alloys

Firstly, the stability of CoCrNi without SRO is studied. To eliminate the error caused by size effect on the phase stability, we constructed a 54-atom SAE configuration for fcc CoCrNi solid solution [42], *i.e.*,  $3 \times 3 \times 3$  hcp supercell for hcp solid solution and  $3 \times 3 \times 2$  fcc  $\langle 111 \rangle$  supercell for fcc solid solution. **Fig. 5** shows the energy of hcp and fcc solid solution with different magnetic states. We can find that the hcp phase is more stable than fcc at different magnetic states. In fact, when CoCrNi is considered as a fully disordered solid solution, the calculated results based on CPA and SQS all suggested that fcc is not the ground state structure, with respect to the double hexagonal close packed (dhcp) and hcp phases [43]. Considering that the size of SAE structure for CoCrNi is slightly small, we constructed three SAE configurations for hcp and fcc phases, respectively. Note that the fcc SAE structures are based on the fcc  $\langle 111 \rangle$  configuration (ABC stacked hexagonal structure). For the hcp or fcc SAE structures, the difference of energy per atom between three SAE configurations is smaller than  $5 \times 10^{-3}$  eV/atom for the same magnetic state.

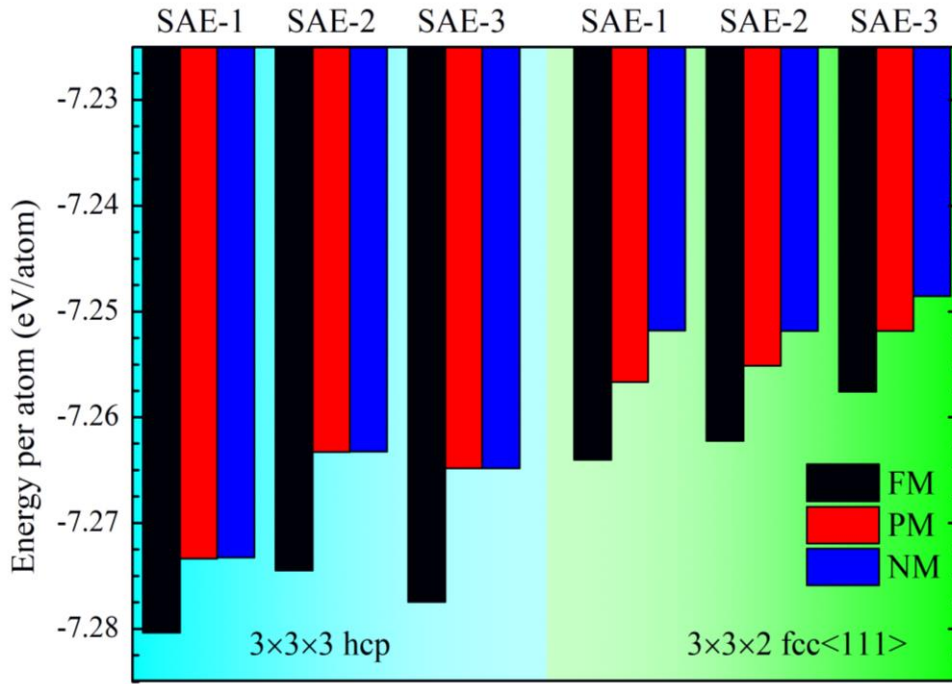


**Fig. 5.** Average energy per atom  $E$  (eV/atom) of the random CoCrNi solid solution at different magnetic states. SAE-1, SAE-2 and SAE-3 represent the three SAE configurations with 54 atoms for hcp and for fcc<111> phases. FM, PM and NM represent the ferromagnetic, paramagnetic and non magnetic states, respectively.

Secondly, the stability of CoCrNi with SRO is studied. Recent experiments indicated that there is SRO near Cr atoms (close to  $(\text{Ni,Co})_2\text{Cr}$ ) in the fcc CoCrNi alloy [44]. In our SAE structural model, the new SRO parameter is introduced as a constraint for the consideration of the SRO. **Fig. 6** shows the illustrated distribution of the first nearest neighboring atom pairs near one Cr atom. For the fully disordered CoCrNi alloy, the SRO parameter  $\theta$  should be equal to 1 for each atom pair. For the CoCrNi with SRO (near Cr), there are less Cr atoms in the first nearest neighbors of Cr atoms, so the value of  $\theta_2^1(\text{Cr, Cr})$  should be smaller than 1. During the structural modeling, the minimum and maximum values for the SRO parameter  $\theta_2^1(\text{Cr, Cr})$  are 0.75 and 0.825 respectively. **Fig. 7** shows the radial distribution of the nearest neighboring atom pairs for the CoCrNi solid solution with SRO. For the 1NN atom pairs, the number of Cr-Ni and Cr-Co is 88 and 92, respectively, whereas the number of Cr-Cr is 60. The SRO in the model structure is obvious. Meanwhile, similar neighboring distribution is kept for the 2NN~5NN atom pairs.

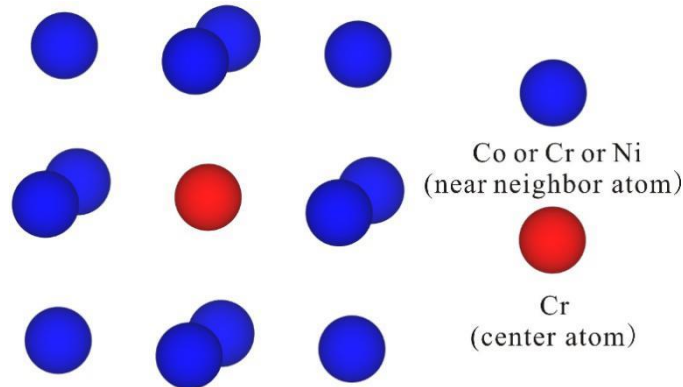


**Fig.6.** Illustrative configuration of the CoCrNi alloy with SRO.

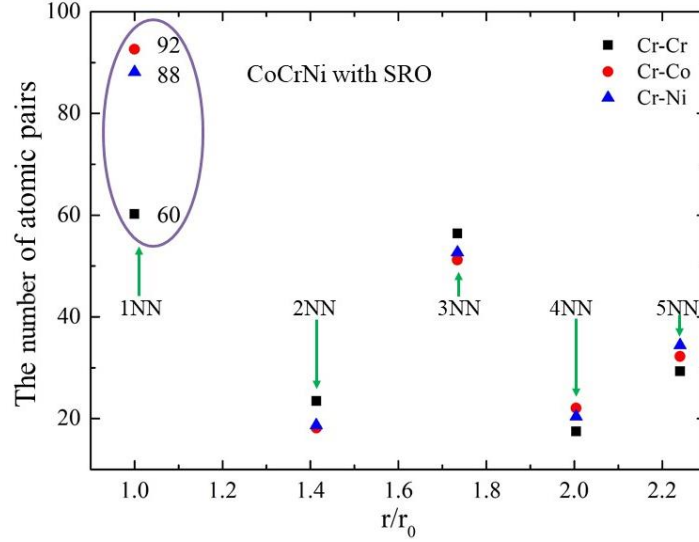


**Fig. 7.** The number of the  $N$ th ( $N=1-5$ ) nearest neighboring (NN) atom pairs for CoCrNi with SRO.  $r_0$  is the first neighboring atom distance.

**Table 4** Equilibrium volume per atom  $V$  ( $\text{\AA}^3$ ), average energy per atom  $E$  (eV/atom), and magnetic moment per atom  $\mu$  ( $\mu_B$ ) for SAE structures for CoCrNi with/without SRO, respectively. There are 108 atoms in each SAE structure. FM, PM and NM represent the ferromagnetic, paramagnetic and non-magnetic states, respectively.

SAE	fcc SAE with SRO			fcc SAE without SRO		
	$V$	$E$	$\mu$	$V$	$E$	$\mu$
1(FM)	10.89	-7.27308	0.380	10.96	-7.25780	0.516
1(PM)	10.88	-7.27222	0.090	10.94	-7.25507	0.226
1(NM)	10.82	-7.27003	0	10.85	-7.24931	0
2(FM)	10.91	-2.27664	0.431	10.95	-7.25955	0.642
2(PM)	10.89	-7.27458	0.01	10.94	-7.25768	0.357
2(NM)	10.82	-7.27033	0	10.85	-7.25044	0
3(FM)	10.90	-7.27722	0.334	10.95	-7.26018	0.596
3(PM)	10.89	-7.27498	0.01	10.92	-7.25783	0
3(NM)	10.81	-7.27259	0	10.84	-7.25263	0

**Table 4** shows the equilibrium bulk properties of the CoCrNi solid solution with/without SRO. Results suggest that the SRO makes the fcc structure more stable than the hcp phase. Due to the existence of antiferromagnetic Cr atoms, the Curie temperature of CoCrNi is very low ( $<5\text{K}$ ) [19]. According to the available estimation of Curie temperature, our *ab initio* predicted Curie temperature is about 6.8~21.2 K from three different SAE configurations. For the CoCrNi solid solution with SRO, three SAE configurations have similar average magnetic moment close to  $0.4 \mu_B$  at ferromagnetic state, while the average magnetic moment of paramagnetic state is close to zero. Whereas the average magnetic moment of random CoCrNi solid solution is slightly large, with respect to the CoCrNi solid solution with SRO, *i.e.*, SRO induces the decrease of magnetic order. In the three magnetic states, the ferromagnetic state has the largest equilibrium volume. The increasing equilibrium volume of CoCrNi without SRO may derive from the magnetic order.

## V. Conclusion

We have presented a new method for the description of atomic environment (AE) of an atom and introduced the similar atomic environment (SAE) approach for structure modeling of the solid-

solution materials. The SAE approach provides a uniform way to take into account both the full disorder and short-range order via minimizing the objective function in the configuration space. A new type of short-range order parameters based on the concept of atom cluster is introduced, which can provide finer characterization of SRO in solid solution. The SAE method could be applied to analyze the effect of different SRO on the stability of solid solution, providing more details in the structures of real solid solution.

We prove theoretically that the optimal structure generated by the SAE method must be the optimal structure of the special quasi-random structure (SQS) method and find a numerical counterexample to the necessity. Based on the delicate implementation, an effective method based on Metropolis Monte Carlo algorithm is provided for the optimization of the objective function. We are enabled to extend the applicability of SAE method from full disorder to partial disorder and from substitutional solid solution to interstitial one.

It is demonstrated by typical alloy applications that the supercell configurations generated by the SAE method are able to describe the complicated solid-solution alloys. For the CoCrFeMnNi high-entropy alloy composed of multiple magnetic alloying elements, the ferromagnetic, antiferromagnetic and paramagnetic states have very close equilibrium volume and energy, although their average magnetic moments are slightly different. An *ab initio* calculation on Ta-W continued solid-solution binary alloy with partial disorder suggested that Ta-W has the tendency to form ordered B2 phase at 0K. The SRO plays a key role in the phase stability and magnetic order in the CoCrNi medium-entropy alloy.

In general, the SAE method allows investigating the phase transformation from the fully disordered to short-range ordered solid solution based on the free energy calculations. We conclude that the combination of the SAE approach with *ab initio* calculations offers an effective approach to the study on the electronic structure, phase stability and mechanical properties of solid-solution materials.

## Acknowledge

This work was supported by the Science Challenge Project (Grant No. TZ2018002) and the National Key Research and Development Program of China (Grant No. 2016YFB0201204). Authors also acknowledge the National Science Foundation of China (Grant Nos. 51701015, 91730302, 11501039, U1804123).

## Reference

- [1] G. Wrangln, *An Introduction to Corrosion and Protecting of Metals* (Chapman and Hall, New York, 1985).
- [2] J. Sato, T. Omori, K. Oikawa, I. Ohnuma, R. Kainuma, and K. Ishida, *Science* (80-. ). **312**, 90 (2006).
- [3] Z. Lei, X. Liu, H. Wang, Y. Wu, S. Jiang, and Z. Lu, *Scr. Mater.* **165**, 164 (2019).
- [4] R. Liu, H. Chen, K. Zhao, Y. Qin, B. Jiang, T. Zhang, G. Sha, X. Shi, C. Uher, and W. Zhang, *Adv. Mater.* **29**, 1702367 (2017).
- [5] M. Schwarze, W. Tress, B. Beyer, F. Gao, R. Scholz, C. Poelking, K. Ortstein, A. A. Günther, D. Kasemann, D. Andrienko, and K. Leo, in *Science* (80-. ). (2016), pp. 515–527.
- [6] N. Ueno, *Science* (80-. ). **352**, 1395 (2016).
- [7] M. C. Tropicovsky, J. R. Morris, P. R. C. Kent, A. R. Lupini, and G. M. Stocks, *Phys. Rev. X* **5**, 1 (2015).

- [8] P. Hohenberg and W. Kohn, Phys. Rev. **136**, B864 (1964).
- [9] W. Kohn and L. J. Sham, Phys. Rev. **140**, A1133 (1965).
- [10] L. Bellaiche and D. Vanderbilt, Phys. Rev. B **61**, 7877 (2000).
- [11] P. Soven, Phys. Rev. **156**, 809 (1967).
- [12] J. W. D. Connolly and A. R. Williams, Phys. Rev. B **27**, 5169 (1983).
- [13] A. Zunger, S.-H. Wei, L. G. Ferreira, and J. E. Bernard, Phys. Rev. Lett. **65**, 353 (1990).
- [14] C. Jiang, Phys. Rev. Lett. **116**, 105501 (2016).
- [15] A. V Ruban and I. A. Abrikosov, Reports Prog. Phys. **71**, 046501 (2008).
- [16] L. Vitos, *Computational Quantum Mechanics for Materials Engineers: The EMTO Method and Applications* (Springer-Verlag, London, UK, 2007).
- [17] Y. Zhang, T. T. Zuo, Z. Tang, M. C. Gao, K. a. Dahmen, P. K. Liaw, and Z. P. Lu, Prog. Mater. Sci. **61**, 1 (2013).
- [18] Y. Zhang, G. M. Stocks, K. Jin, C. Lu, H. Bei, B. C. Sales, L. Wang, L. K. Béland, R. E. Stoller, G. D. Samolyuk, M. Caro, A. Caro, and W. J. Weber, Nat. Commun. **6**, 8736 (2015).
- [19] K. Jin, B. C. Sales, G. M. Stocks, G. D. Samolyuk, M. Daene, W. J. Weber, Y. Zhang, and H. Bei, Sci. Rep. **6**, 20159 (2016).
- [20] J. Y. He, H. Wang, Y. Wu, X. J. Liu, H. H. Mao, T. G. Nieh, and Z. P. Lu, Intermetallics **79**, 41 (2016).
- [21] D. Choudhuri, T. Alam, T. Borkar, B. Gwalani, A. S. Mantri, S. G. Srinivasan, M. A. Gibson, and R. Banerjee, Scr. Mater. **100**, 36 (2015).
- [22] J. E. Saal and C. Wolverton, Acta Mater. **61**, 2330 (2013).
- [23] F. Tian, L. Delczeg, N. Chen, L. K. Varga, J. Shen, and L. Vitos, Phys. Rev. B **88**, 085128 (2013).
- [24] K. B. Zhang, Z. Y. Fu, J. Y. Zhang, W. M. Wang, H. Wang, Y. C. Wang, Q. J. Zhang, and J. Shi, Mater. Sci. Eng. A **508**, 214 (2009).
- [25] Y.-F. Kao, T.-J. Chen, S.-K. Chen, and J.-W. Yeh, J. Alloys Compd. **488**, 57 (2009).
- [26] W. Guo, W. Dmowski, J.-Y. Noh, P. Rack, P. K. Liaw, and T. Egami, Metall. Mater. Trans. A **44**, 1994 (2012).
- [27] A. Van De Walle, P. Tiwary, M. De Jong, D. L. Olmsted, M. Asta, A. Dick, D. Shin, Y. Wang, L. Q. Chen, and Z. K. Liu, Calphad Comput. Coupling Phase Diagrams Thermochem. **42**, 13 (2013).
- [28] J. M. Sanchez, F. Ducastelle, and D. Gratias, Phys. A Stat. Mech. Its Appl. **128**, 334 (1984).
- [29] A. van de Walle, Nat. Mater. **7**, 455 (2008).
- [30] Y. Zhao, X. Chen, and J. Li, Nano Res. **10**, 3407 (2017).
- [31] D. Wales and J. Doye, J. Phys. Chem. A **5639**, 5111 (1998).
- [32] G. Kresse and M. Marsman, VASP Man. (2014).
- [33] J. P. Perdew, K. Burke, and M. Ernzerhof, Phys. Rev. Lett. **77**, 3865 (1996).
- [34] P. E. Blöchl, Phys. Rev. B **50**, 17953 (1994).
- [35] H. J. Monkhorst and J. D. Pack, Phys. Rev. B **13**, 5188 (1976).
- [36] B. L. Gyorffy, A. J. Pindor, J. Staunton, G. M. Stocks, and H. Winter, J. Phys. F Met. Phys. **15**, 1337 (1985).
- [37] B. Cantor, I. T. H. Chang, P. Knight, and a. J. B. Vincent, Mater. Sci. Eng. A **375–377**, 213 (2004).
- [38] F. Tian, L. K. Varga, J. Shen, and L. Vitos, Comput. Mater. Sci. **111**, 350 (2016).
- [39] D. Ma, B. Grabowski, F. Körmann, J. Neugebauer, and D. Raabe, Acta Mater. **100**, 90 (2015).
- [40] C. L. Tracy, S. Park, D. R. Rittman, S. J. Zinkle, H. Bei, M. Lang, R. C. Ewing, and W. L. Mao, Nat. Commun. **8**, 1 (2017).
- [41] F. Zhang, Y. Wu, H. Lou, Z. Zeng, V. Prakapenka, E. Greenberg, and Y. Ren, Nat. Commun. **8**, 1 (2017).
- [42] B. Gludovatz, A. Hohenwarter, K. V. S. Thurston, H. Bei, Z. Wu, E. P. George, and R. O. Ritchie, Nat. Commun. **7**, 10602 (2016).

- [43] Z. Z. Zhang, H. Sheng, Z. Wang, B. Gludovatz, Z. Z. Zhang, E. P. George, Q. Yu, S. X. Mao, and R. O. Ritchie, *Nat. Commun.* **8**, 14390 (2017).
- [44] F. X. Zhang, S. Zhao, K. Jin, H. Xue, G. Velisa, H. Bei, R. Huang, J. Y. P. Ko, D. C. Pagan, J. C. Neufeind, W. J. Weber, and Y. Zhang, *Phys. Rev. Lett.* **118**, 205501 (2017).